


Communication

# Photoluminescence and Energy Transfer in Double- and Triple-Lanthanide-Doped $\text{YVO}_4$ Nanoparticles

Vassiliy A. Medvedev<sup>1</sup>, Ilya E. Kolesnikov<sup>2</sup>, Pavel K. Olshin<sup>3</sup>, Mikhail D. Mikhailov<sup>4</sup>, Alina A. Manshina<sup>1,\*</sup>   
and Daria V. Mamonova<sup>1,\*</sup>

<sup>1</sup> Institute of Chemistry, Saint Petersburg State University, Saint Petersburg 199034, Russia; st063851@student.spbu.ru

<sup>2</sup> Centre for Optical and Laser Materials Research, Research Park, Saint Petersburg State University, Saint Petersburg 198504, Russia; ilya-kolesnikov@mail.ru

<sup>3</sup> School of Natural science, Ulsan National Institute of Science and Technology, Ulsan 44919, Korea; pavel\_olshin@bk.ru

<sup>4</sup> High School of Physics of Materials and Technologies, Peter the Great St. Petersburg Polytechnic University, Saint Petersburg 195251, Russia; mikhail.sudoma@yandex.ru

\* Correspondence: a.manshina@spbu.ru (A.A.M.); magwicher@gmail.com (D.V.M.)

**Abstract:** Optical materials doped with several lanthanides are unique in their properties and are widely used in various fields of science and technology. The study of these systems provides solutions for noncontact thermometry, bioimaging, sensing technology, and others. In this paper, we report on the demonstration of  $\text{YVO}_4$  nanoparticles doped with one, two, and three different rare earth ions ( $\text{Tm}^{3+}$ ,  $\text{Er}^{3+}$ , and  $\text{Nd}^{3+}$ ). We discuss the morphology, structural properties, and luminescence behavior of particles. Luminescence decay kinetics reveal the energy transfer efficiency (up to 78%) for different ions under the selective excitation of individual ions. Thus, we found that the energy transition from  $\text{Tm}^{3+}$  is more favorable than from  $\text{Er}^{3+}$  while we did not observe any significant energy rearrangement in the samples under the excitation of  $\text{Nd}^{3+}$ . The observed strong variation of REI lifetimes makes the suggested nanoparticles promising for luminescent labeling, anticounterfeiting, development of data storage systems, etc.

**Keywords:** oxide nanoparticles; luminescence kinetics; rare earth ions; codoped systems



**Citation:** Medvedev, V.A.; Kolesnikov, I.E.; Olshin, P.K.; Mikhailov, M.D.; Manshina, A.A.; Mamonova, D.V. Photoluminescence and Energy Transfer in Double- and Triple-Lanthanide-Doped  $\text{YVO}_4$  Nanoparticles. *Materials* **2022**, *15*, 2637. <https://doi.org/10.3390/ma15072637>

Academic Editors: Valerio Pinchetti and Sergei Kulinich

Received: 11 February 2022

Accepted: 1 April 2022

Published: 3 April 2022

**Publisher's Note:** MDPI stays neutral with regard to jurisdictional claims in published maps and institutional affiliations.



**Copyright:** © 2022 by the authors. Licensee MDPI, Basel, Switzerland. This article is an open access article distributed under the terms and conditions of the Creative Commons Attribution (CC BY) license (<https://creativecommons.org/licenses/by/4.0/>).

## 1. Introduction

The combination of different types of rare earth ions (REI) in a single structure (single crystals, ceramics, glass ceramics, hybrid nanomaterials, etc.) represents a unique optical system, in which the luminescent properties can be tuned in a wide range by controlling the energy transfer between ions of different types through adjusting the composition and structure of the material. Such sophisticated optical systems can find applications in different fields, including ultrabroadband optical devices [1–3], microthermometry [4–6], bioimaging [7–10], and the production of light-emitting flexible materials [11–13].

To date, the optical properties of all rare earth ions are well studied, and luminescence properties of individual ions in different media are thoroughly described. However, the combination of several REI in one crystalline host can completely change the optical properties of the materials due to the energy transfer between the ions. Moreover, the luminescence behavior of these substances strongly depends on the types of REI, their concentrations, the type of the matrix, and the excitation mechanism. It is noteworthy that the effect of each of these parameters requires special consideration.

Metal oxides demonstrate several advantages for selection as the host for the REI doping. First, they are characterized by the stability of the physical and chemical behavior over a wide temperature range, biocompatibility, and mechanical hardness. The

combination of these properties makes them promising candidates for a wide range of applications in mechanical engineering [14–16], medicine [17,18], sensing technology [19,20], anticounterfeiting [21,22], and others [23,24].

Many of these applications are based on the kinetic luminescence parameters that are unique for each specimen containing a different combination of ions. For example, luminescence coding indicators based on luminescence lifetimes, color spatial distribution, and intensity ratio between emission bands have been demonstrated to find multiple applications in different fields, such as bioimaging, deep tissue multiplexing labelling/detection, high-density data storage, and anticounterfeiting [25–27]. The temperature dependence of the kinetic parameters of oxide particles doped with REI can be used for luminescence nanothermometry [28,29].

Recently, we have reported on the synthesis and luminescence properties of  $\text{YVO}_4:\text{Tm}^{3+}$ ,  $\text{Er}^{3+}$ , and  $\text{Nd}^{3+}$  particles [30]. We selected these ions because of the absence of the overlapping luminescence bands, which makes it possible to study the direct energy transfer between the ions. In this paper, we demonstrate  $\text{YVO}_4$  nanoparticles doped not only with one or three but also with combinations of two different REI. Nanoparticles codoped with several ions were obtained thanks to adjusting the synthesis procedure—a modified Pechini method. The luminescence kinetics of the proposed optical system was studied in detail. Altogether, it provided a demonstration of the highly efficient energy transfer processes in codoped nanoparticles of  $\text{YVO}_4$  and a strong variation of REI lifetimes that is of great importance for luminescent labeling, anticounterfeiting, development of data storage systems, etc.

## 2. Materials and Methods

The particles were synthesized with the modified Pechini method that is described in detail in our previous paper [31]. Water solutions of yttrium and REI nitrates and vanadium oxide were used as initial reagents. Citric acid was chosen as the chelating agent to prepare a mixture of citrate complexes. Then, we added ethylene glycol to the solution to form a polymer gel with all metal ions within a cross-linked network. After this, we annealed the gel at 550 °C to decompose the complexes to the oxides (or complex oxides). It resulted in the formation of small particles that are characterized by a large number of defects. To solve this issue, we performed a high temperature (900 °C, 1 h) calcination of the mixture following the addition of KCl (the mass ratio 2:1 to the mass of the oxide particles) to the products of the previous stage of the reaction. This additional reaction step led to the formation of weakly agglomerated particles with a high degree of crystallinity. After the thermal treatment, we removed the potassium chloride with distilled water.

Table 1 demonstrates the composition of the particles that we synthesized for further experiments. We prepared single-, double-, and triple-doped particles to thoroughly study the energy transfer between the ions and unravel its mechanism. The concentrations of each individual REI were selected separately and kept constant in all samples. It is known that increasing the REI concentration leads to a gradual increase of the luminescence intensity until concentration quenching starts, which results in a luminescence decrease at a higher concentration range of REI. This time, we increased the concentrations of the  $\text{Tm}^{3+}$  and  $\text{Er}^{3+}$  ions in the  $\text{YVO}_4$  samples to 1.0 and 3.0 at %, respectively, to enhance the luminescence intensity of these ions relative to the most intense emission band of the  $\text{Nd}^{3+}$  ions.

The structure of the samples was characterized with X-ray diffraction (XRD) using a Bruker “D8 DISCOVER” operating with a  $\text{CuK}\alpha$  line (1.54056 Å). The crystal unit cell parameters and the coherent scattering region size were calculated using TOPAS software. The morphology of the powders was studied with scanning electron microscopy (SEM Zeiss Supra 40VP, Zeiss, Oberkochen, Germany); the size distribution of the particles in aqueous dispersions was analyzed with the static light scattering (SLS) method (Mastersizer 3000, Malvern Instruments Ltd, Malvern, Worcestershire, UK). The optical absorption spectra and luminescence properties of the samples were measured with a

Lambda 1050 spectrophotometer and Horiba Jobin Yvon Fluorolog-3 spectrofluorimeter with a Xe-arc lamp (450 W power), respectively.

**Table 1.** Compositions of the crystalline particles.

№	Combinations of Rare Earth Ions	Concentration, at. %		
		Tm	Er	Nd
1	YVO <sub>4</sub> :Nd <sup>3+</sup>	-	-	0.03
2	YVO <sub>4</sub> :Er <sup>3+</sup>	-	3.0	-
3	YVO <sub>4</sub> :Tm <sup>3+</sup>	1.0	-	-
4	YVO <sub>4</sub> :Tm <sup>3+</sup> , Er <sup>3+</sup>	1.0	3.0	-
5	YVO <sub>4</sub> :Tm <sup>3+</sup> , Nd <sup>3+</sup>	1.0	-	0.03
6	YVO <sub>4</sub> :Er <sup>3+</sup> , Nd <sup>3+</sup>	-	3.0	0.03
7	YVO <sub>4</sub> :Tm <sup>3+</sup> , Er <sup>3+</sup> , Nd <sup>3+</sup>	1.0	3.0	0.03

### 3. Results and Discussion

#### 3.1. Structure and Morphology

According to the X-ray diffraction analysis, all synthesized samples consist of an yttrium vanadate crystalline phase with a tetragonal structure (JCPDS 17-0341). Figure 1a shows several representative diffraction patterns of single-, double-, and triple-doped particles. The proper purification of the particles from potassium chloride after heat treatment in the salt melt is confirmed by the absence of KCl lines located at 28.3 and 40.5 degrees (JCPDS 04-0587). The coherent scattering region of all samples lies in a narrow range between 60–80 nm as the synthesis conditions were identical. However, the doping of the oxide crystalline host with the REI affects the unit cell parameters (Figure 1b) as the ionic radius of Y<sup>3+</sup> (0.090 nm) is larger than that of erbium Er<sup>3+</sup> (0.089 nm) and Tm<sup>3+</sup> (0.088 nm) but smaller than the ionic radius of Nd<sup>3+</sup> (0.098 nm). The smallest cell volume belongs to the triple-doped YVO<sub>4</sub> as it contains an increased concentration of substitution ions with a smaller ionic radius (Er<sup>3+</sup> and Tm<sup>3+</sup>).

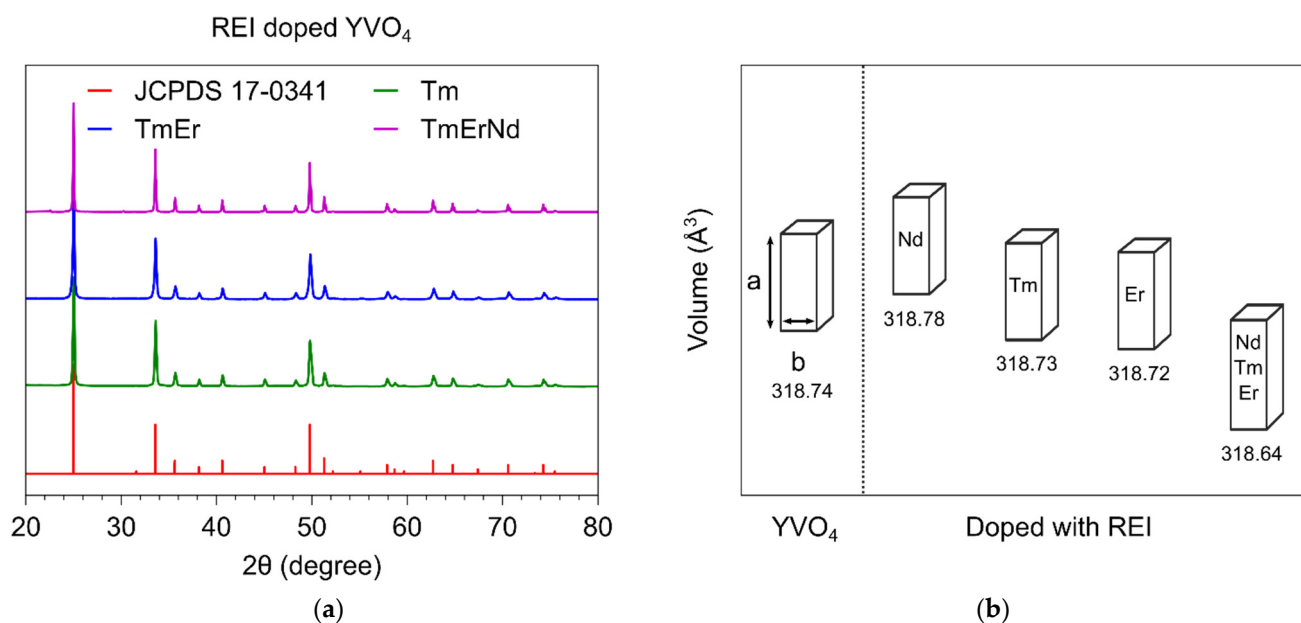


**Figure 1.** (a) XRD patterns and (b) unit cell volume of the YVO<sub>4</sub> samples doped with different rare earth ions.

Figure 2 demonstrates the morphology and the size distribution of the prepared particles. According to the SEM images (Figure 2a), the individual particles (with the size

that rarely exceeds 100 nm) often possess an octahedral shape, which differs from that of the previously synthesized particles and is due to the higher volume of the salt melt (KCl) during the second stage of the heat treatment. This is also confirmed by the results of the SLS (Figure 2b) of the  $\text{YVO}_4$  powder in the aqueous solution. The experimental results propose a unimodal distribution of the particles with the average size of  $\sim 50$  nm.

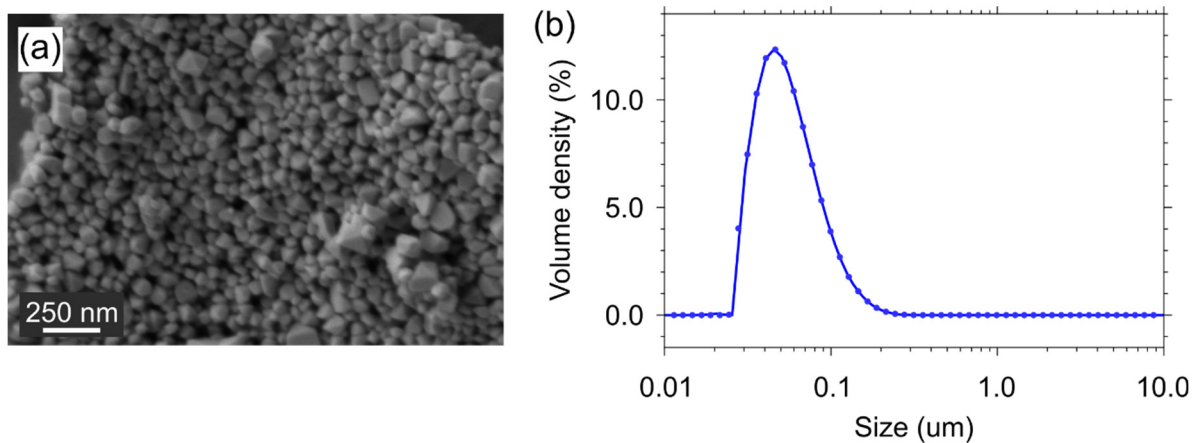


**Figure 2.** (a) SEM image and (b) size distribution of the triple-doped  $\text{YVO}_4$ :  $\text{Nd}^{3+}$ ,  $\text{Er}^{3+}$ , and  $\text{Tm}^{3+}$  particles.

### 3.2. Luminescence Properties

The direct excitation of REI makes it possible to study the probability of energy transfer between different rare earth ions in the same host. For this purpose, the specific excitation wavelength for each REI has been chosen. Figure 3a presents an optical absorption spectrum of pure  $\text{YVO}_4$ . The broad peak centered around 310 nm is attributed to the direct absorption of the  $\text{YVO}_4$  host, namely to the charge transfer from the oxygen ligands to the central vanadium atom inside the  $\text{VO}_4^{3-}$  ion [32]. Excitation at this wavelength results in the simultaneous emission of all doping REI through the energy transfer from the crystalline host (Figure 3b,c) and significantly complicates the study of the energy transfer between ions. The excitation spectra were recorded at the most intense NIR emission lines of each dopant ion, 1064 nm, 857 nm, and 800 nm for  $\text{Nd}^{3+}$ ,  $\text{Er}^{3+}$ , and  $\text{Tm}^{3+}$ , respectively. From the obtained spectra, several lines for the selective excitation of ions of each type,  $^4\text{I}_{9/2} - ^4\text{G}_{5/2} + ^4\text{G}_{7/2}$  (595 nm) for  $\text{Nd}^{3+}$ ,  $^4\text{I}_{15/2} - ^2\text{H}_{11/2}$  (526 nm) for  $\text{Er}^{3+}$ , and  $^3\text{H}_4 - ^3\text{F}_2 + ^3\text{F}_3$  (692 nm) for  $\text{Tm}^{3+}$ , were found.

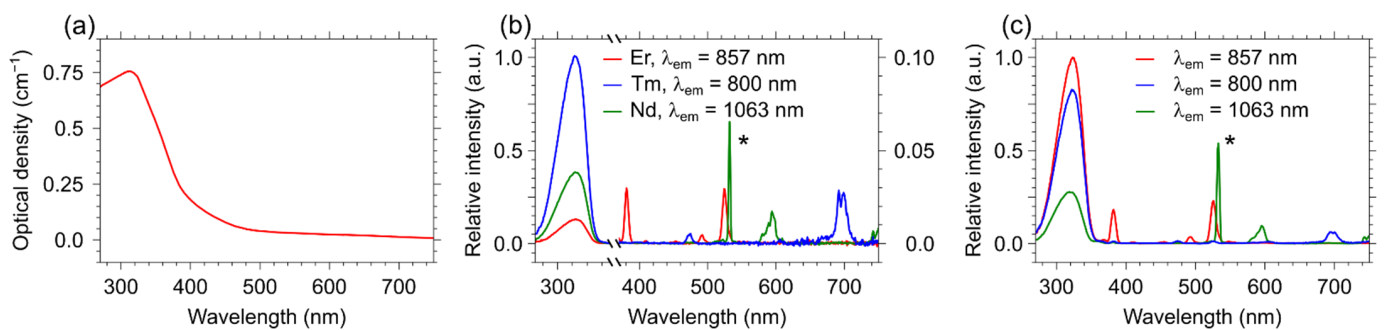


**Figure 3.** (a) Optical absorption spectra of pure  $\text{YVO}_4$  particles; (b) excitation spectra of the single-doped  $\text{YVO}_4$ :  $\text{Nd}^{3+}$  (0.03 at.%),  $\text{YVO}_4$ :  $\text{Er}^{3+}$  (3 at.%), and  $\text{YVO}_4$ :  $\text{Tm}^{3+}$  (1 at.%) samples and (c) triple-doped  $\text{YVO}_4$ :  $\text{Nd}^{3+}$  (0.03 at.%),  $\text{Er}^{3+}$  (3 at.%), and  $\text{Tm}^{3+}$  (1 at.%) samples monitored at different wavelengths  $\lambda_{\text{em}} = 1064$ , 857, and 800 nm corresponding to the luminescence emission bands of Nd, Er, and Tm, respectively. The asterisk (\*) indicates the second order of diffraction.

Steady-state emission and luminescence kinetics are discussed individually for each ion that can act as a donor. Figure 4a shows the emission spectra of all samples containing

erbium ions. The emission spectrum of the single-doped  $\text{YVO}_4: \text{Er}^{3+}$  (3 at.%) sample consists of  $^4\text{S}_{3/2} - ^4\text{I}_{13/2}$  (857 nm) and  $^4\text{I}_{11/2} - ^4\text{I}_{15/2}$  (986 nm) transitions. Codoping  $\text{YVO}_4: \text{Er}^{3+}$  with another ion ( $\text{Tm}^{3+}$  or  $\text{Nd}^{3+}$ ) in the structure produces spectra with characteristic lines of both ions:  $^3\text{H}_4 - ^3\text{H}_6$  (800 nm) for  $\text{Tm}^{3+}$  and  $^4\text{F}_{3/2} - ^4\text{I}_{9/2}$  (882 nm) for  $\text{Nd}^{3+}$ . Since selective erbium excitation was used ( $\lambda_{\text{ex}} = 526 \text{ nm}$ ), this indicates an energy transfer between the active centres in the double-doped samples. The triple-doped sample demonstrates a simultaneous energy transfer from erbium to  $\text{Nd}^{3+}$  and  $\text{Tm}^{3+}$ . From the analysis of the emission spectra for single-, double-, and triple-doped samples, we proposed an energy transfer scheme, which reflects the occurring processes upon the direct excitation of  $\text{Er}^{3+}$  ions (Figure 4b).

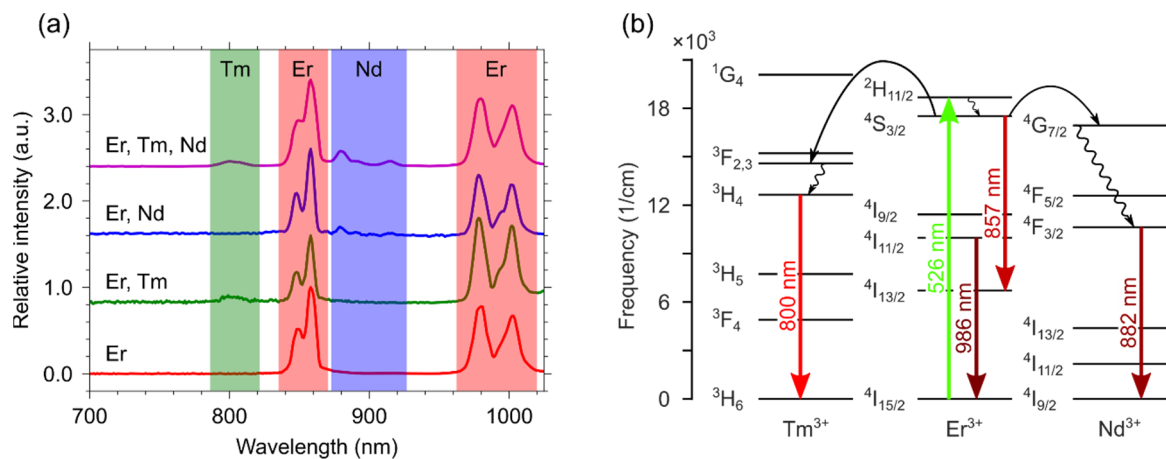


**Figure 4.** (a) Emission spectra and (b) scheme of energy migrations between ions for the single-, double-, and triple-doped  $\text{YVO}_4: \text{Nd}^{3+}$  (0.03 at.%),  $\text{Er}^{3+}$  (3 at.%), and  $\text{Tm}^{3+}$  (1 at.%) samples under excitation with  $\lambda_{\text{ex}} = 526 \text{ nm}$ .

Figure 5 shows the decay curves of erbium-containing samples monitored at the erbium  $^4\text{S}_{3/2} - ^4\text{I}_{15/2}$  transition ( $\lambda_{\text{em}} = 553 \text{ nm}$ ,  $\lambda_{\text{ex}} = 526 \text{ nm}$ ). It is noteworthy that the luminescence decay curves started from  $50 \mu\text{s}$ , but for the clear representation of the data, we shifted some datasets along the x-axis. The experimental data were fitted by a single exponential function:  $I = I_0 \cdot e^{-t/\tau}$ , where  $\tau$  is the observed lifetime of the  $^4\text{S}_{3/2}$  level. Due to the energy transfer in the double- and triple-doped samples, the luminescence lifetime decreases from  $7.96 \pm 0.13 \mu\text{s}$  ( $\text{YVO}_4: \text{Er}^{3+}$ ) to  $7.15 \pm 0.15 \mu\text{s}$  ( $\text{YVO}_4: \text{Er}^{3+}, \text{Tm}^{3+}$ ) and  $6.64 \pm 0.20 \mu\text{s}$  ( $\text{YVO}_4: \text{Nd}^{3+}, \text{Er}^{3+}, \text{Tm}^{3+}$ ). We do not observe a decrease in the lifetime for the  $\text{YVO}_4: \text{Er}^{3+}, \text{Nd}^{3+}$  sample due to the low concentration of  $\text{Nd}^{3+}$ .

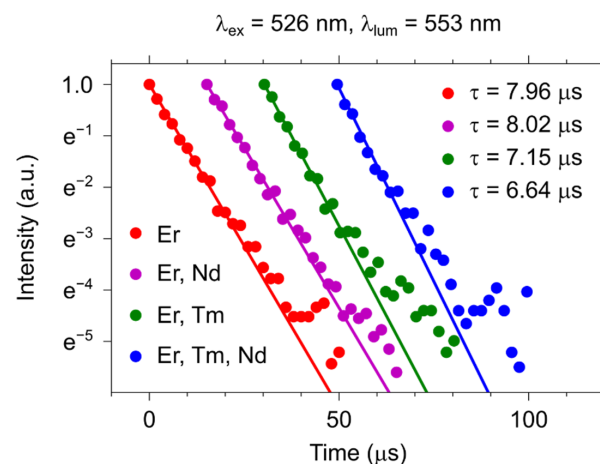


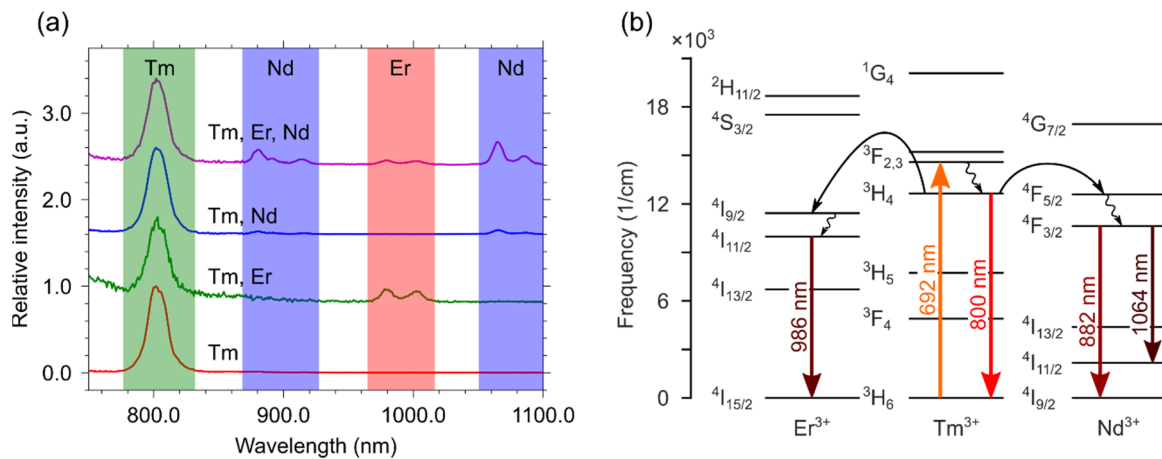
**Figure 5.** Luminescence decay curves of the one-, two-, and three-doped samples with the selective excitation of  $\text{Er}^{3+}$  ions.

The energy transfer efficiency ( $\eta$ ) for the erbium-containing samples has been calculated using the following formula:  $\eta = \left(1 - \frac{\tau_{da}}{\tau_d}\right) \times 100\%$ , where  $\tau_{da}$  is the donor lifetime in the presence of the acceptor and  $\tau_d$  is the unquenched donor lifetime (Table 2) [33,34]. In the double-doped  $\text{Nd}^{3+}$ ,  $\text{Er}^{3+}$  sample, the energy transfer efficiency is zero due to the low concentration of neodymium. However, this low concentration in the triple-doped sample gives a contribution to the energy transfer efficiency as this value in the double-doped  $\text{Er}^{3+}$ ,  $\text{Tm}^{3+}$  sample is lower ( $\eta = 10\%$ ) than in the triple-doped sample ( $\eta = 17\%$ ).

**Table 2.** Values of energy transfer efficiency for one-, two-, and triple-doped systems with the selective excitation of  $\text{Er}^{3+}$  ions.

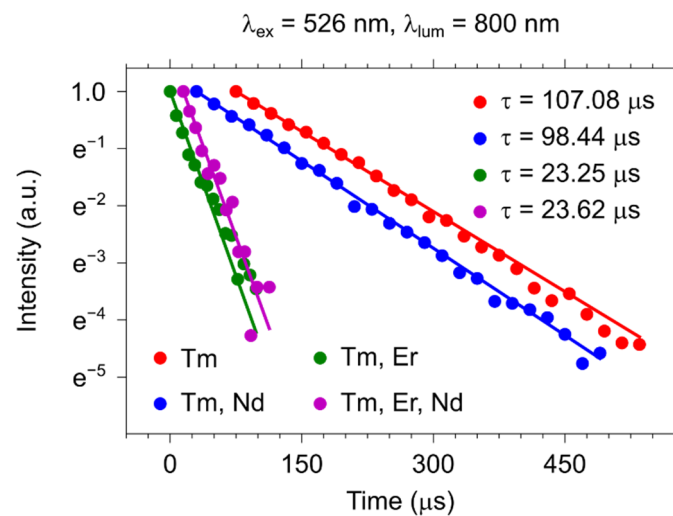
$\eta$ , %	Combination of $\text{Er}^{3+}$ Ions		
	$\text{Er}^{3+}$ , $\text{Tm}^{3+}$ , $\text{Nd}^{3+}$	$\text{Er}^{3+}$ , $\text{Tm}^{3+}$	$\text{Er}^{3+}$ , $\text{Nd}^{3+}$
	17	10	0

Figure 6a displays the emission spectra of all samples containing thulium ions. The emission spectrum of the single-doped  $\text{YVO}_4:\text{Tm}^{3+}$  (1 at.%) sample demonstrates a strong  ${}^3\text{H}_4 - {}^3\text{H}_6$  (800 nm) transition. The introduction of the second ion ( $\text{Er}^{3+}$  or  $\text{Nd}^{3+}$ ) in the structure leads to the appearance of characteristic lines of the corresponding ion, namely  ${}^4\text{S}_{3/2} - {}^4\text{I}_{13/2}$  (857 nm) and  ${}^4\text{I}_{11/2} - {}^4\text{I}_{15/2}$  (986 nm) transitions for  $\text{Er}^{3+}$  and  ${}^4\text{F}_{3/2} - {}^4\text{I}_{9/2}$  (882 nm) and  ${}^4\text{F}_{3/2} - {}^4\text{I}_{11/2}$  (1064 nm) transitions for  $\text{Nd}^{3+}$ . Since we selectively excite ( $\lambda_{\text{ex}} = 692$  nm), this indicates a strong energy transfer between the active ions in the double-doped samples. Similarly, the triple-doped sample shows emission bands attributed to all three ions. Based on the analysis of the luminescence spectra for single-, double- and triple-doped samples, we suggest an energy transfer scheme following the direct excitation of  $\text{Tm}^{3+}$  (Figure 6b).



**Figure 6.** (a) Emission spectra and (b) scheme of energy migrations between ions for the single-, double-, and triple-doped  $\text{YVO}_4:\text{Nd}^{3+}$  (0.03 at.%),  $\text{Er}^{3+}$  (3 at.%), and  $\text{Tm}^{3+}$  (1 at.%) samples under excitation with  $\lambda_{\text{ex}} = 692$  nm.

In Figure 7, we show the luminescence lifetimes of the  $\text{YVO}_4$  particles doped with  $\text{Tm}^{3+}$  and other REI monitored at the thulium  ${}^3\text{H}_4 - {}^3\text{H}_6$  transition ( $\lambda_{\text{em}} = 800$  nm) under direct excitation ( $\lambda_{\text{ex}} = 692$  nm). Unlikely to the  $\text{Er}^{3+}$  lifetime, the addition of a small fraction of  $\text{Nd}^{3+}$  ions leads to a noticeable variation in the  ${}^3\text{H}_4$  lifetime ( $\sim 9\%$ ). However, the presence of  $\text{Er}^{3+}$  ions in the double- and triple-doped samples drastically accelerates the quenching of the transition, and the lifetime reaches almost  $23 \mu\text{s}$  for both cases. This fact is probably explained by a low energy mismatch of the  $\text{Tm}^{3+}$  and  $\text{Er}^{3+}$  excited levels, which results in an efficient  $\text{Tm}^{3+} - \text{Er}^{3+}$  energy transfer.



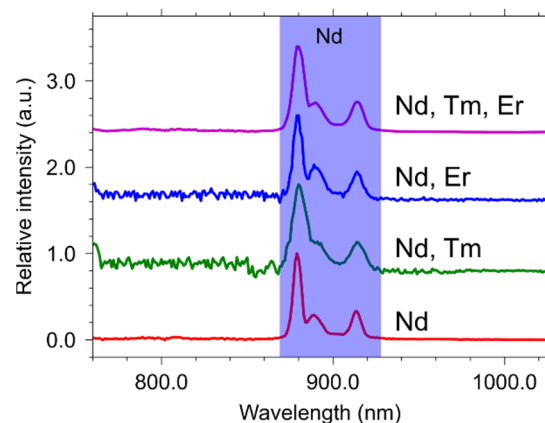
**Figure 7.** Luminescence decay curves of one-, two-, and triple-doped samples with the selective excitation of  $\text{Tm}^{3+}$  ions.

Table 3 has the values of energy transfer efficiency for the thulium-containing samples. In the double-doped  $\text{Nd}^{3+}$ ,  $\text{Tm}^{3+}$  nanoparticles, the efficiency reaches 8%. The sample containing  $\text{Tm}^{3+}$  and  $\text{Er}^{3+}$  ions showed the highest values of energy transfer efficiency ( $\eta = 78\%$ ) among the studied compositions.

**Table 3.** Values of energy transfer efficiency for the one-, two-, and triple-doped systems with the selective excitation of  $\text{Tm}^{3+}$  ions.

$\eta$ , %	Combination of $\text{Tm}^{3+}$ Ions		
	$\text{Er}^{3+}$ , $\text{Tm}^{3+}$ , $\text{Nd}^{3+}$	$\text{Er}^{3+}$ , $\text{Tm}^{3+}$	$\text{Tm}^{3+}$ , $\text{Nd}^{3+}$
	78	78	8

The emission spectrum of the single-doped  $\text{YVO}_4: \text{Nd}^{3+}$  (0.03 at.%) sample displays peaks assigned to the  ${}^4\text{F}_{3/2} - {}^4\text{I}_{9/2}$  transition (882 nm). The same emission lines are observed in the double- and triple-doped samples (Figure 8). The low concentration of neodymium in combination with the low energy transfer efficiency could explain the absence of erbium and thulium lines in the emission spectra when neodymium is directly excited.



**Figure 8.** Emission spectra for the single-, double-, and triple-doped  $\text{YVO}_4: \text{Nd}^{3+}$  (0.03 at.%),  $\text{Er}^{3+}$  (3 at.%), and  $\text{Tm}^{3+}$  (1 at.%) samples under excitation with  $\lambda_{\text{ex}} = 595$  nm.

#### 4. Conclusions

In this work, we studied the energy transfer in nanocrystalline yttrium vanadate particles doped with different combinations of three ion types ( $\text{Er}^{3+}$ ,  $\text{Tm}^{3+}$ ,  $\text{Nd}^{3+}$ ). The nanoparticles were synthesized by the modified Pechini method. The powders are characterized by a high degree of crystallinity with an average size of the CSR in the range of 60–80 nm with the majority of the particles below 100 nm. The powders have weak agglomeration and can be transferred into a water solution. Luminescence spectra of all samples were studied upon the direct excitation of each ion ( $\lambda_{\text{ex}} = 526$  nm, 692 nm, and 595 nm for  $\text{Er}^{3+}$ ,  $\text{Tm}^{3+}$ , and  $\text{Nd}^{3+}$ , respectively). From the analysis of characteristic emission lines, we determined the energy transfer between the different ion types in the double- and triple-doped samples. The luminescence kinetics are presented for the group of Er-containing samples and the group of Tm-containing samples under direct excitation into absorption bands of  $\text{Er}^{3+}$  and  $\text{Tm}^{3+}$ , respectively. We found that the thulium ion displays a more efficient energy transfer than the erbium ion. The efficiency increases with the appearance of the third doping ion as an additional pathway for the donor's energy transfer. The small energy transfer efficiency in binary systems with neodymium as the second ion are caused by the low concentration of this ion—a small number of ions causes the same low probability of energy transfer to them, and the high luminescence of neodymium ions ensures the presence of characteristic emission lines in the luminescence spectrum even at such low concentrations.

The demonstrated variability of the luminescence spectra and decay lifetimes at different excitation wavelengths for double- and triple- doped nanoparticles is promising for nanothermometry and systems of spectral encoding based on the ratio of different optical parameters. In such a way, nanoparticles of a simple structure, chemical composition, and morphology demonstrate the advantage in comparison with complicated core–shell multilayer structures.

**Author Contributions:** Conceptualization, D.V.M. and I.E.K.; synthesis V.A.M.; methodology, D.V.M. and I.E.K.; validation, D.V.M., I.E.K. and P.K.O.; formal analysis, V.A.M.; investigation, V.A.M.; data curation, D.V.M. and I.E.K.; writing—original draft preparation, V.A.M. and D.V.M.; writing—review and editing, P.K.O., I.E.K. and A.A.M.; visualization, P.K.O.; supervision, M.D.M. and A.A.M.; project administration, D.V.M.; funding acquisition, D.V.M. All authors have read and agreed to the published version of the manuscript.

**Funding:** This research was funded by the Russian Science Foundation, grant number 20-79-00101.

**Institutional Review Board Statement:** Not applicable.

**Informed Consent Statement:** Not applicable.

**Data Availability Statement:** Not applicable.

**Acknowledgments:** Authors are grateful to the “Interdisciplinary Resource Centre for Nanotechnology”, “Innovative Technologies of Composite Nanomaterials”, “Research Centre for X-ray Diffraction Studies”, and “Centre for Optical and Laser Materials Research” of Saint-Petersburg State University Research Park.

**Conflicts of Interest:** The authors declare no conflict of interest. The funders had no role in the design of the study; in the collection, analyses, or interpretation of data; in the writing of the manuscript; or in the decision to publish the results.

#### References

1. Cesaria, M.; Di Bartolo, B. Chapter 3 Nanophosphors: From Rare Earth Activated Multicolor-Tuning to New Efficient White Light Sources. In *Quantum Nano-Photonics*; Di Bartolo, B., Silvestri, L., Cesaria, M., Collins, J., Eds.; NATO Science for Peace and Security Series B: Physics and Biophysics; Springer: Dordrecht, The Netherlands, 2018; pp. 27–77; ISBN 978-94-024-1543-8.
2. Zhu, Y.; Shen, X.; Zhou, M.; Su, X.; Li, J.; Yang, G.; Shao, H.; Zhou, Y. Ultra-Broadband 1.0 Mm Band Emission Spectroscopy in  $\text{Pr}^{3+}/\text{Nd}^{3+}/\text{Yb}^{3+}$  Tri-Doped Tellurite Glass. *Spectrochim. Acta A* **2019**, *222*, 117178. [[CrossRef](#)] [[PubMed](#)]
3. Son, D.H.; Kim, B.H.; Lee, S.H.; Boo, S.; Han, W.-T. Ultra-Broadband near-Infrared Emission in Bismuth Borosilicate Glasses Incorporated with  $\text{Er}^{3+}$ ,  $\text{Tm}^{3+}$ , and  $\text{Yb}^{3+}$  Ions. *J. Non-Cryst. Solids* **2014**, *402*, 106–110. [[CrossRef](#)]



4. Zhao, D.; Yue, D.; Zhang, L.; Jiang, K.; Qian, G. Cryogenic Luminescent Tb/Eu-MOF Thermometer Based on a Fluorine-Modified Tetracarboxylate Ligand. *Inorg. Chem.* **2018**, *57*, 12596–12602. [[CrossRef](#)] [[PubMed](#)]
5. Kolesnikov, I.E.; Kurochkin, M.A.; Kalinichev, A.A.; Kolesnikov, E.Y.; Lähderanta, E. Optical Temperature Sensing in Tm<sup>3+</sup>/Yb<sup>3+</sup>-Doped GeO<sub>2</sub>-PbO-PbF<sub>2</sub> Glass Ceramics Based on Ratiometric and Spectral Line Position Approaches. *Sens. Actuator A Phys.* **2018**, *284*, 251–259. [[CrossRef](#)]
6. Kolesnikov, I.E.; Afanaseva, E.V.; Kurochkin, M.A.; Vaishlia, E.I.; Kalinichev, A.A.; Kolesnikov, E.Y.; Lähderanta, E. Upconverting NIR-to-NIR LuVO<sub>4</sub>:Nd<sup>3+</sup>/Yb<sup>3+</sup> Nanophosphors for High-Sensitivity Optical Thermometry. *ACS Appl. Mater. Interfaces* **2022**, *14*, 1757–1764. [[CrossRef](#)] [[PubMed](#)]
7. Lv, Y.; Zhou, Z.; Shen, Y.; Zhou, Q.; Ji, J.; Liu, S.; Zhang, Y. Coupled Fluorometer-Potentiostat System and Metal-Free Monochromatic Luminophores for High-Resolution Wavelength-Resolved Electrochemiluminescent Multiplex Bioassay. *ACS Sens.* **2018**, *3*, 1362–1367. [[CrossRef](#)]
8. Yu, S.; Tu, D.; Lian, W.; Xu, J.; Chen, X. Lanthanide-Doped near-Infrared II Luminescent Nanoprobes for Bioapplications. *Sci. China Mater.* **2019**, *62*, 1071–1086. [[CrossRef](#)]
9. Huang, P.; Zheng, W.; Gong, Z.; You, W.; Wei, J.; Chen, X. Rare Earth Ion- and Transition Metal Ion-Doped Inorganic Luminescent Nanocrystals: From Fundamentals to Biodetection. *Mater. Today Nano* **2019**, *5*, 100031. [[CrossRef](#)]
10. Zan, G.; Wu, T.; Zhu, F.; He, P.; Cheng, Y.; Chai, S.; Wang, Y.; Huang, X.; Zhang, W.; Wan, Y.; et al. A Biomimetic Conductive Super-Foldable Material. *Matter* **2021**, *4*, 3232–3247. [[CrossRef](#)]
11. Zhang, L.; Lyu, S.; Chen, Z.; Wang, S. Fabrication Flexible and Luminescent Nanofibrillated Cellulose Films with Modified SrAl<sub>2</sub>O<sub>4</sub>: Eu, Dy Phosphors via Nanoscale Silica and Aminosilane. *Nanomaterials* **2018**, *8*, 352. [[CrossRef](#)]
12. Watanabe, S.; Asanuma, T.; Hyodo, H.; Soga, K.; Matsumoto, M. Micromolding in Capillaries for Calcination-Free Fabrication of Flexible Inorganic Phosphor Films Consisting of Rare-Earth-Ion-Doped Nanoparticles. *Langmuir* **2013**, *29*, 11185–11191. [[CrossRef](#)] [[PubMed](#)]
13. Tran, T.N.L.; Szczurek, A.; Varas, S.; Armellini, C.; Scotognella, F.; Chiasera, A.; Ferrari, M.; Righini, G.C.; Lukowiak, A. Rare-Earth Activated SnO<sub>2</sub> Photoluminescent Thin Films on Flexible Glass: Synthesis, Deposition and Characterization. *Opt. Mater.* **2022**, *124*, 111978. [[CrossRef](#)]
14. Reddy, A.A.; Goel, A.; Tulyaganov, D.U.; Sardo, M.; Mafra, L.; Pascual, M.J.; Kharton, V.V.; Tsipis, E.V.; Kolotygin, V.A.; Ferreira, J.M.F. Thermal and Mechanical Stability of Lanthanide-Containing Glass-Ceramic Sealants for Solid Oxide Fuel Cells. *J. Mater. Chem. A* **2014**, *2*, 1834–1846. [[CrossRef](#)]
15. Matovic, B.; Maletaskic, J.; Zagorac, J.; Pavkov, V.; Maki, R.S.S.; Yoshida, K.; Yano, T. Synthesis and Characterization of Pyrochlore Lanthanide (Pr, Sm) Zirconate Ceramics. *J. Eur. Ceram. Soc.* **2020**, *40*, 2652–2657. [[CrossRef](#)]
16. Chen, L.; Guo, J.; Zhu, Y.; Hu, M.; Feng, J. Features of Crystal Structures and Thermo-mechanical Properties of Weberites RE<sub>3</sub>NbO<sub>7</sub> (RE=La, Nd, Sm, Eu, Gd) Ceramics. *J. Am. Ceram. Soc.* **2021**, *104*, 404–412. [[CrossRef](#)]
17. Zhang, X.; Huang, Y.; Wang, B.; Chang, X.; Yang, H.; Lan, J.; Wang, S.; Qiao, H.; Lin, H.; Han, S.; et al. A Functionalized Sm/Sr Doped TiO<sub>2</sub> Nanotube Array on Titanium Implant Enables Exceptional Bone-Implant Integration and Also Self-Antibacterial Activity. *Ceram. Int.* **2020**, *46*, 14796–14807. [[CrossRef](#)]
18. Jinga, S.-I.; Anghel, A.-M.; Brincoveanu, S.-F.; Bucur, R.-M.; Florea, A.-D.; Saftau, B.-I.; Stroe, S.-C.; Zamfirescu, A.-I.; Busuioc, C. Ce/Sm/Sr-Incorporating Ceramic Scaffolds Obtained via Sol-Gel Route. *Materials* **2021**, *14*, 1532. [[CrossRef](#)]
19. Benali, A.; Azizi, S.; Bejar, M.; Dhahri, E.; Graça, M.F.P. Structural, Electrical and Ethanol Sensing Properties of Double-Doping LaFeO<sub>3</sub> Perovskite Oxides. *Ceram. Int.* **2014**, *40*, 14367–14373. [[CrossRef](#)]
20. Hossain, M.K.; Ahmed, M.H.; Khan, M.I.; Miah, M.S.; Hossain, S. Recent Progress of Rare Earth Oxides for Sensor, Detector, and Electronic Device Applications: A Review. *ACS Appl. Electron. Mater.* **2021**, *3*, 4255–4283. [[CrossRef](#)]
21. Pei, P.; Wei, R.; Wang, B.; Su, J.; Zhang, Z.; Liu, W. An Advanced Tunable Multimodal Luminescent La<sub>4</sub>GeO<sub>8</sub>: Eu<sup>2+</sup>, Er<sup>3+</sup> Phosphor for Multicolor Anticounterfeiting. *Adv. Funct. Mater.* **2021**, *31*, 2102479. [[CrossRef](#)]
22. Pujales-Paradela, R.; Granath, T.; Seuffert, M.T.; Kasper, T.; Müller-Buschbaum, K.; Mandel, K. Luminescent Magnets: Hybrid Supraparticles of a Lanthanide-Based MOF and Ferromagnetic Iron Oxide by Assembly in a Droplet via Spray-Drying. *J. Mater. Chem. C* **2022**, *10*, 1017–1028. [[CrossRef](#)]
23. Al-Qahtani, S.D.; Binyaseen, A.M.; Aljuhani, E.; Aljohani, M.; Alzahrani, H.K.; Shah, R.; El-Metwaly, N.M. Production of Smart Nanocomposite for Glass Coating toward Photochromic and Long-Persistent Photoluminescent Smart Windows. *Ceram. Int.* **2022**, *48*, 903–912. [[CrossRef](#)]
24. Ghosh, K.; Murshed, M.M.; Frederichs, T.; Muniraju, N.K.C.; Gesing, T.M. Structural, Vibrational, Thermal, and Magnetic Properties of Mullite-type NdMnTiO<sub>5</sub> Ceramic. *J. Am. Ceram. Soc.* **2022**, *105*, 2702–2712. [[CrossRef](#)]
25. Zhou, L.; Fan, Y.; Wang, R.; Li, X.; Fan, L.; Zhang, F. High-Capacity Upconversion Wavelength and Lifetime Binary Encoding for Multiplexed Biodetection. *Angew. Chem.* **2018**, *130*, 13006–13011. [[CrossRef](#)]
26. Liu, H.; Jayakumar, M.K.G.; Huang, K.; Wang, Z.; Zheng, X.; Ågren, H.; Zhang, Y. Phase Angle Encoded Upconversion Luminescent Nanocrystals for Multiplexing Applications. *Nanoscale* **2017**, *9*, 1676–1686. [[CrossRef](#)]
27. Zhang, F.; Haushalter, R.C.; Haushalter, R.W.; Shi, Y.; Zhang, Y.; Ding, K.; Zhao, D.; Stucky, G.D. Rare-Earth Upconverting Nanobarcodes for Multiplexed Biological Detection. *Small* **2011**, *7*, 1972–1976. [[CrossRef](#)]
28. Gharouel, S.; Labrador-Páez, L.; Haro-González, P.; Horchani-Naifer, K.; Férid, M. Fluorescence Intensity Ratio and Lifetime Thermometry of Praseodymium Phosphates for Temperature Sensing. *J. Lumin.* **2018**, *201*, 372–383. [[CrossRef](#)]

29. Kolesnikov, I.; Manshina, A. Rare Earth Ion Based Luminescence Thermometry. In *Progress in Photon Science*; Yamanouchi, K., Manshina, A.A., Makarov, V.A., Eds.; Springer Series in Chemical Physics; Springer: Cham, Switzerland, 2021; Volume 125, pp. 69–94; ISBN 978-3-030-77645-9.
30. Medvedev, V.A.; Mamonova, D.V.; Kolesnikov, I.E.; Khokhlova, A.R.; Mikhailov, M.D.; Manshina, A.A. Synthesis and Luminescence Properties of  $\text{YVO}_4$ :  $\text{Nd}^{3+}$ ,  $\text{Er}^{3+}$  and  $\text{Tm}^{3+}$  Nanoparticles. *Inorg. Chem. Commun.* **2020**, *118*, 107990. [[CrossRef](#)]
31. Kolesnikov, I.E.; Lvanova, T.Y.; Ivanov, D.A.; Kireev, A.A.; Mamonova, D.V.; Golyeva, E.V.; Mikhailov, M.D.; Manshina, A.A. In-Situ Laser-Induced Synthesis of Associated  $\text{YVO}_4$ : $\text{Eu}^{3+}$ @ $\text{SiO}_2$ @Au-Ag/C Nanohybrids with Enhanced Luminescence. *J. Solid State Chem.* **2018**, *258*, 835–840. [[CrossRef](#)]
32. Singh, N.; Mugesh, G.  $\text{CeVO}_4$  Nanozymes Catalyze the Reduction of Dioxygen to Water without Releasing Partially Reduced Oxygen Species. *Angew. Chem.* **2019**, *131*, 7879–7883. [[CrossRef](#)]
33. Paulose, P.I.; Jose, G.; Thomas, V.; Unnikrishnan, N.V.; Warriar, M.K.R. Sensitized Fluorescence of  $\text{Ce}^{3+}$  / $\text{Mn}^{2+}$  System in Phosphate Glass. *J. Phys. Chem. Solids* **2003**, *64*, 841–846. [[CrossRef](#)]
34. Kolesnikov, I.E.; Mamonova, D.V.; Kurochkin, M.A.; Kolesnikov, E.Y.; Lähderanta, E.; Manshina, A.A.  $\text{YVO}_4$  Nanoparticles Doped with  $\text{Eu}^{3+}$  and  $\text{Nd}^{3+}$  for Optical Nanothermometry. *ACS Appl. Nano Mater.* **2021**, *4*, 12481–12489. [[CrossRef](#)]